Electronic Supplementary Material (ESI) for CrystEngComm

Supporting Information

Exploration and Synthesis of Condensed Coordination Networks with modified Magnetic Properties

Susanne Wöhlert [a], Lothar Fink[b], Martin Schmidt[b] and Christian Näther*[a]

*[a] Institut für Anorganische Chemie, Christian-Albrechts-Universität zu Kiel, Max-Eyth-Straße 2, 24118 Kiel, Germany. Fax: +49 431-880 1520; Tel: +49 431-880 1520; *E-mail:cnaether@ac.uni-kiel.de*
[b] Institut für Anorganische und Analytische Chemie, Johann Wolfgang Goethe Universität, Max-von-Laue-Str. 7, 60438 Frankfurt am Main.

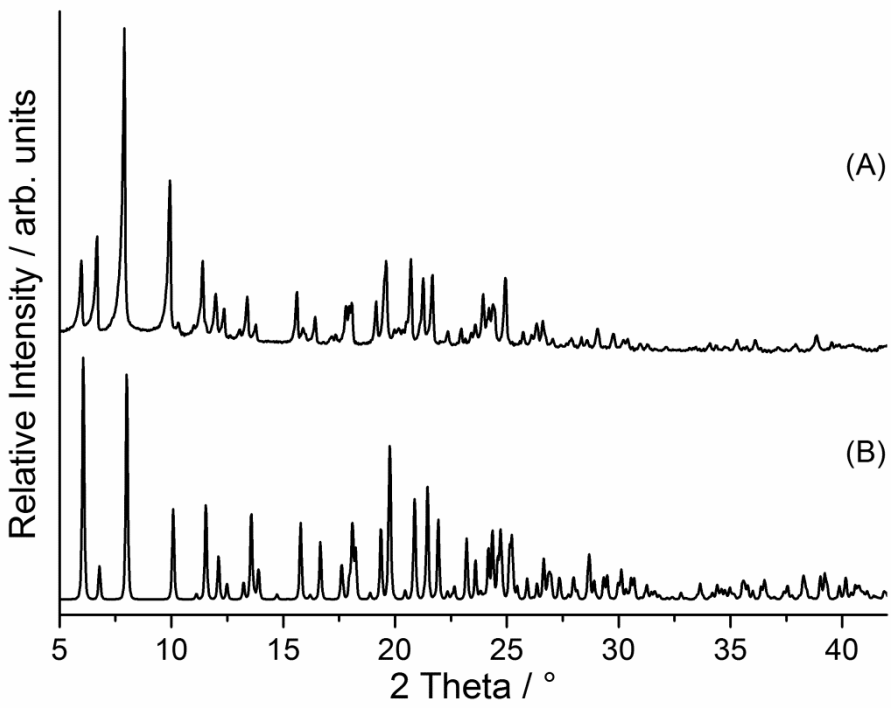

Figure S1. Experimental XRPD of **2** (A) and calculated XRPD from single-crystal data of $Ni(NCS)_2(2\text{-methylpyrazine})_4 \cdot 2\text{-methylpyrazine}$ solvate (**2**) (B).

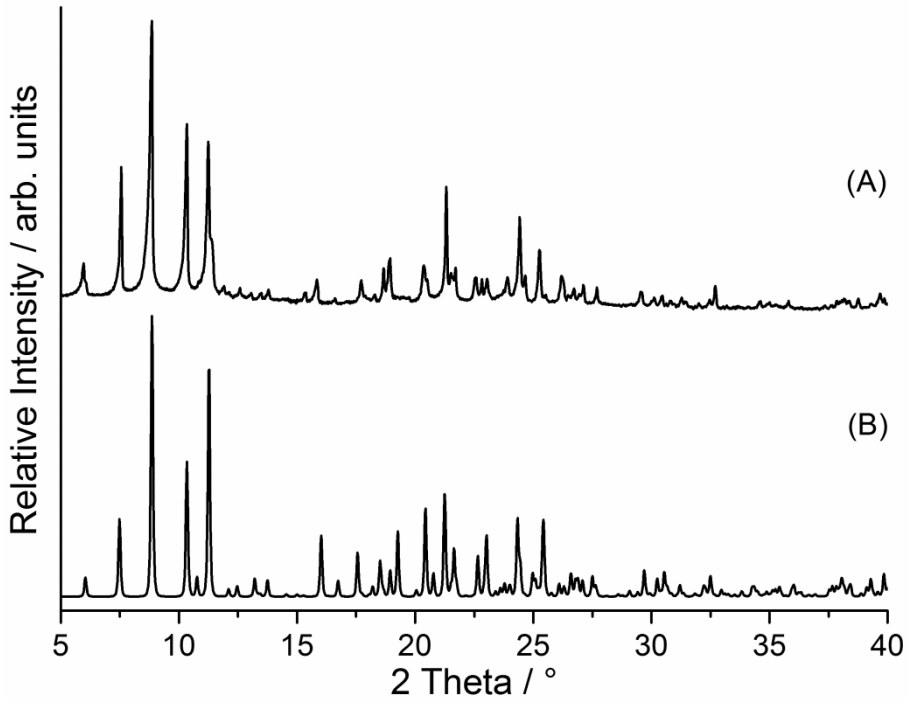

Figure S2. Experimental XRPD of **3** (A) and calculated XRPD from single-crystal data of $Ni(NCS)_2(2\text{-methylpyrazine})_4 \cdot \text{ethanol}$ solvate (**3**) (B).

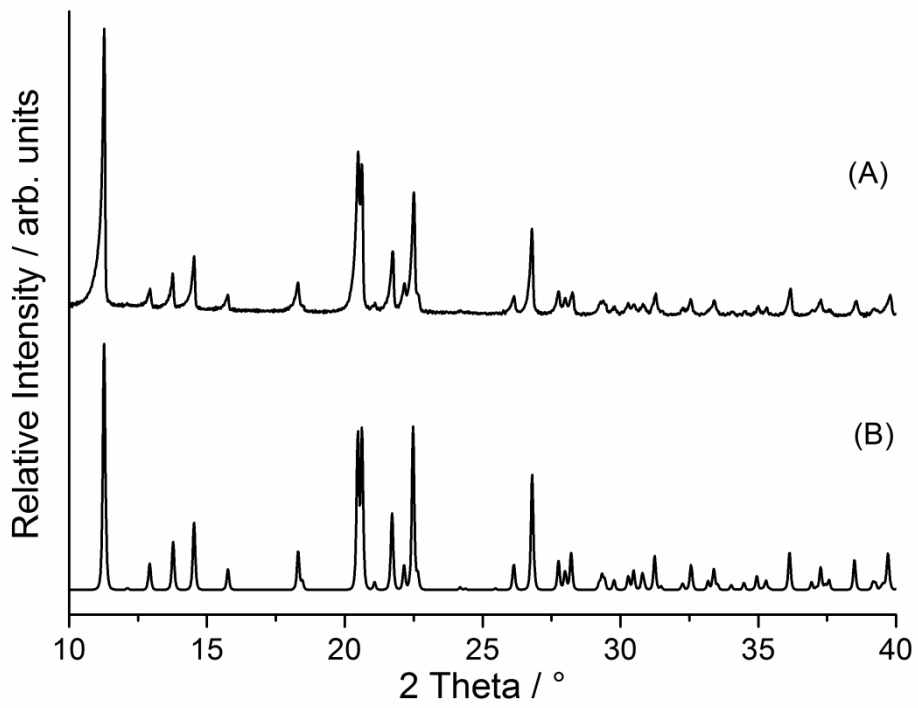

Figure S3. Experimental XRPD of **4** (A) and calculated XRPD for the literature known compound $Ni(NCS)_2(2\text{-methylpyrazine})_2(H_2O)_2$ (**4**) (B).

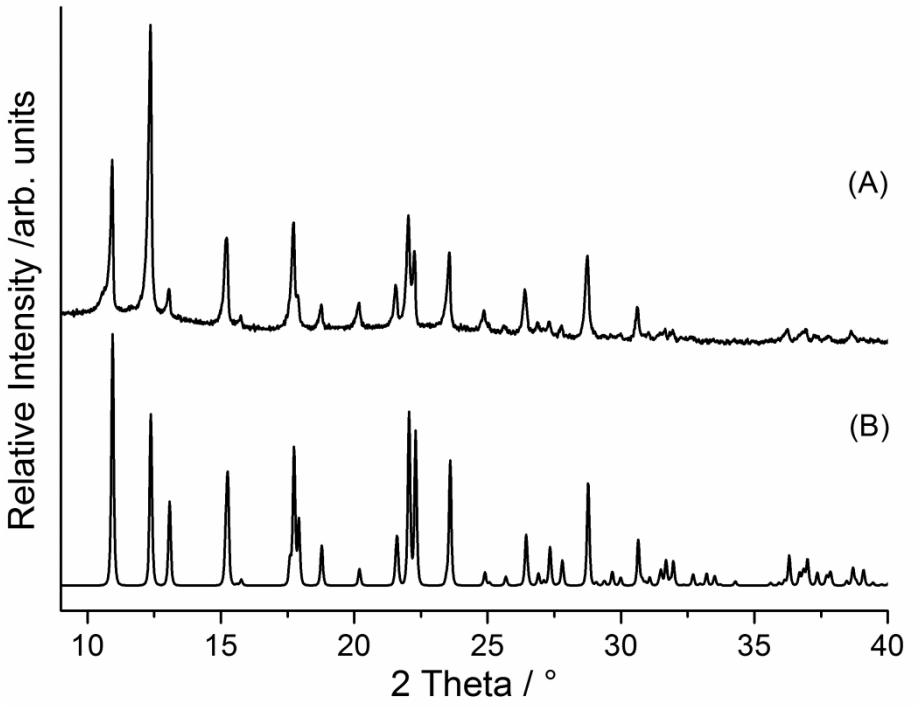

Figure S4. Experimental XRPD of **5** (A) and calculated XRPD from single-crystal data of $Ni(NCS)_2(2\text{-methylpyrazine})_2(CH_3OH)_2$ (**5**) (B).

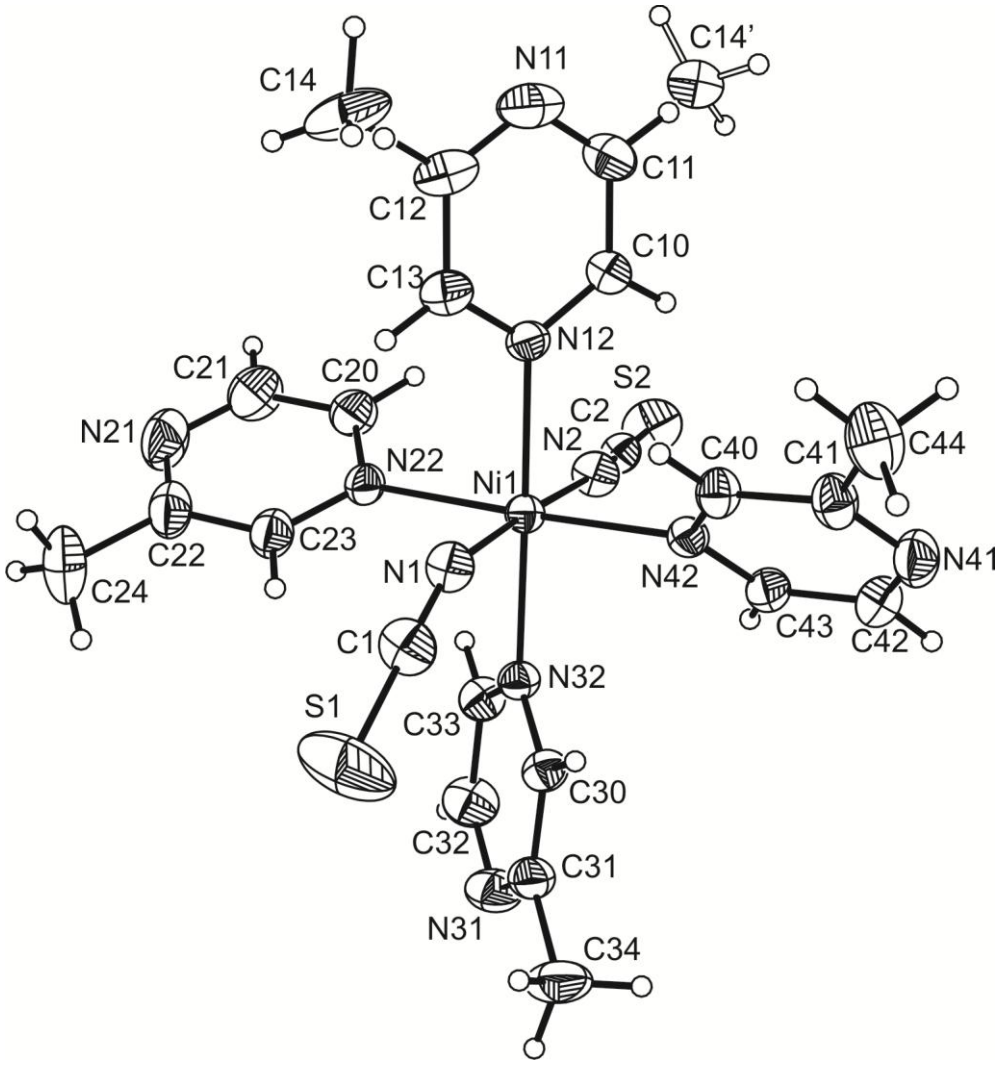

Figure S5. Crystal structure of $Ni(NCS)_2(2\text{-methylpyrazine})_4$ (**1**) with view of the coordination sphere of the nickel(II) cation with labeling and displacement ellipsoids drawn at 50 % probability level.

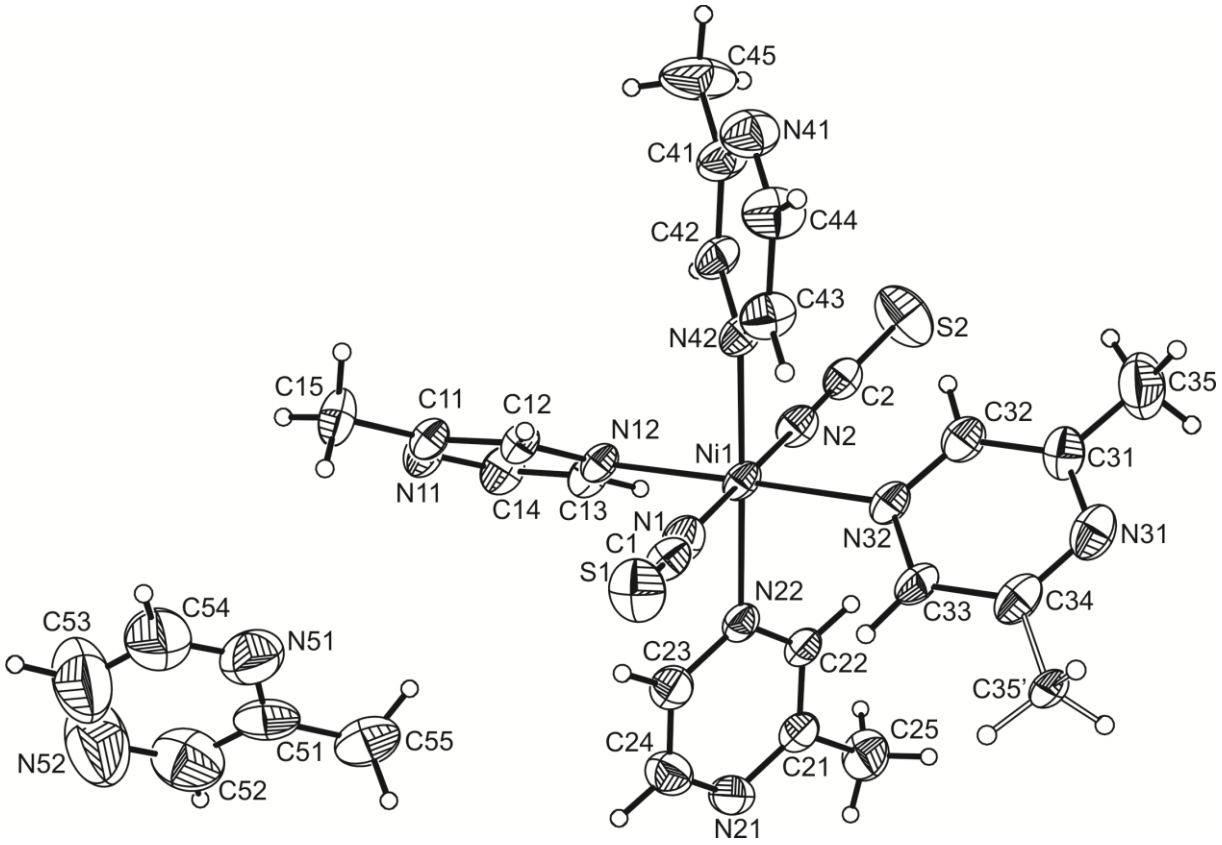

Figure S6. Crystal structure of $Ni(NCS)_2(2\text{-methylpyrazine})_4 \cdot 2\text{-methylpyrazine}$ solvate (**2**) with view of the coordination sphere of the nickel(II) cation with labeling and displacement ellipsoids drawn at 50 % probability level.

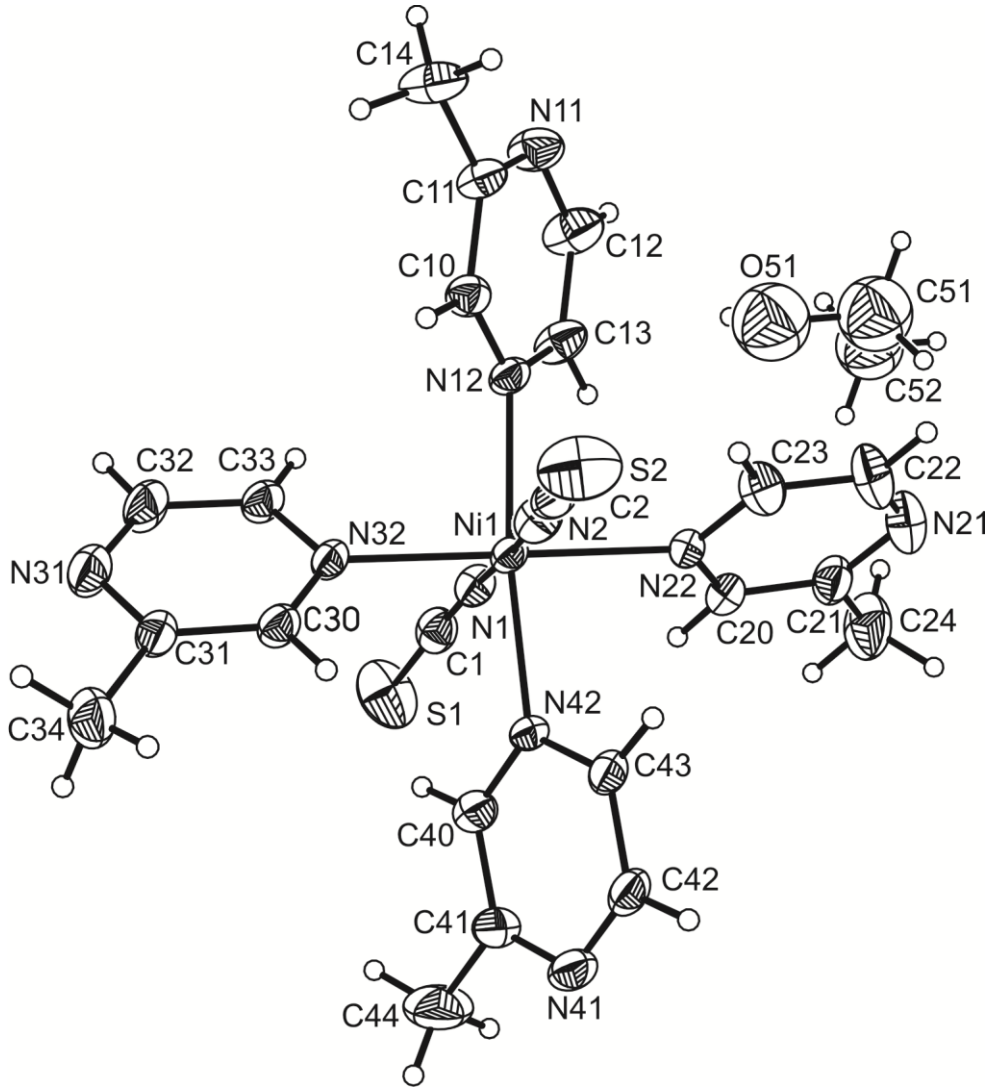

Figure S7. Crystal structure of $Ni(NCS)_2(2\text{-methylpyrazine})_4 \cdot$ethanol solvate (**3**) with view of the coordination sphere of the nickel(II) cation with labeling and displacement ellipsoids drawn at 50 % probability level.

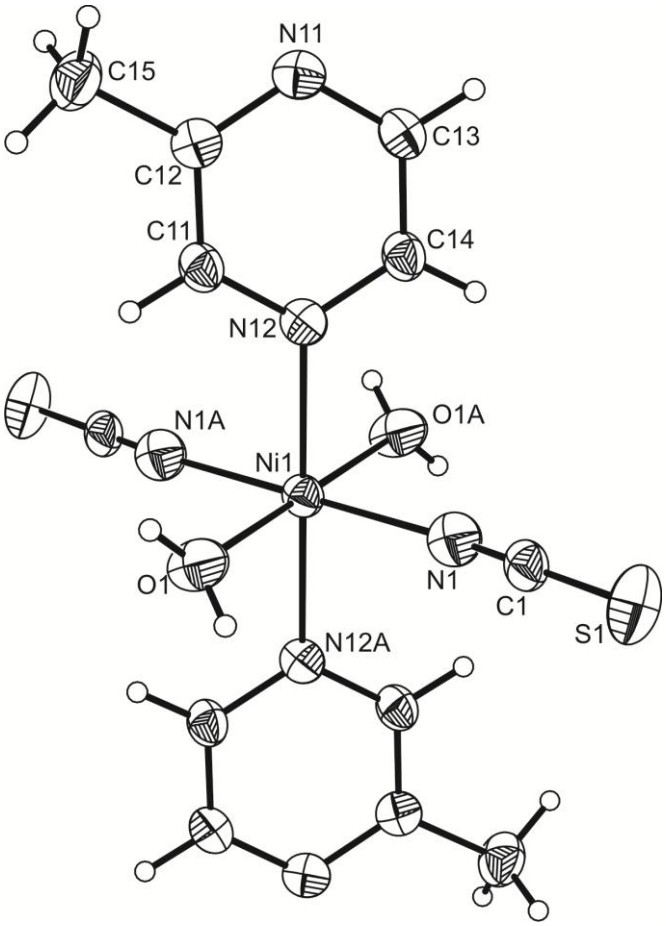

Figure S8. Crystal structure of $Ni(NCS)_2(2\text{-methylpyrazine})_2(H_2O)_2$ (**4**) with view of the coordination sphere of the nickel(II) cation with labeling and displacement ellipsoids drawn at 50 % probability level. Symmetry code: A = -x, -y, -z + 1.

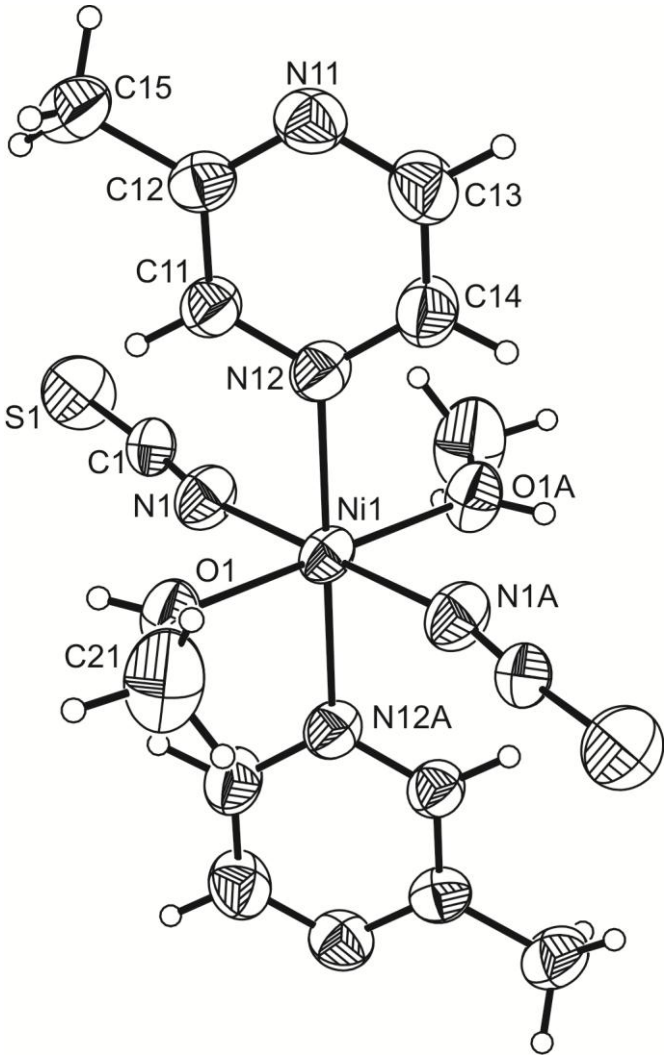

Figure S9. Crystal structure of $Ni(NCS)_2(2\text{-methylpyrazine})_2(CH_3OH)_2$ (**5**) with view of the coordination sphere of the nickel(II) cation with labeling and displacement ellipsoids drawn at 50 % probability level. Symmetry code: A = -x + 1, -y + 1, -z.

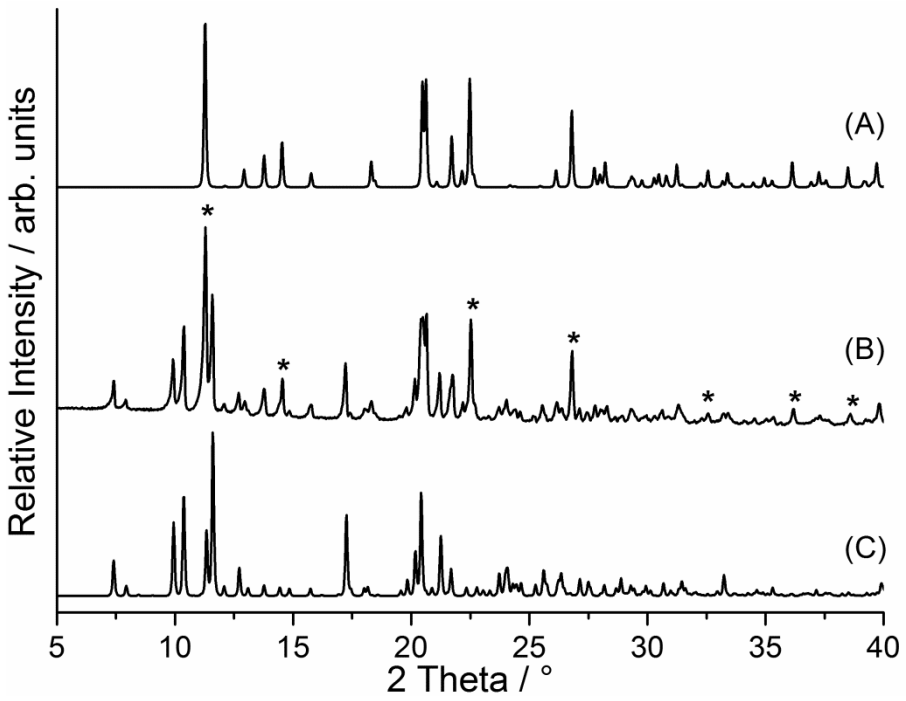

Figure S10. Experimental XRPD of **6** (B) (the reflections of the 1:2:2 compound $Ni(NCS)_2(2\text{-methylpyrazine})_2(H_2O)_2$ (**4**) are indicated by stars) and calculated XRPD from single-crystal data of $[Ni(NCS)_2(2\text{-methylpyrazine})_4 \cdot Ni(NCS)_2(2\text{-methylpyrazine})_3(H_2O)]$ (**6**; C) together with the calculated XRPD from single-crystal data of $Ni(NCS)_2(2\text{-methylpyrazine})_2(H_2O)_2$ (**4**; A).

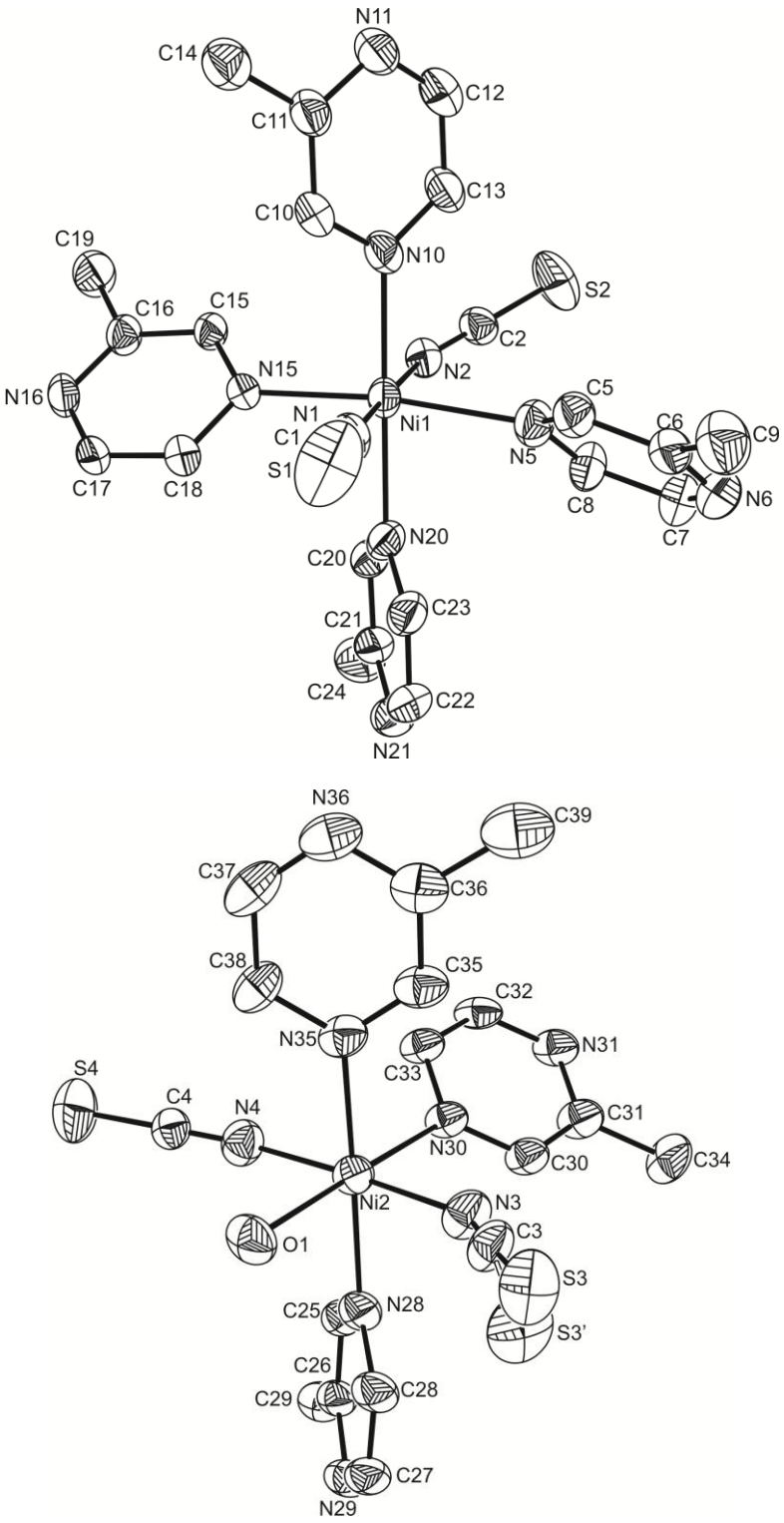

Figure S11. Crystal structure of $[Ni(NCS)_2(2\text{-methylpyrazine})_4 \cdot Ni(NCS)_2(2\text{-methylpyrazine})_3(H_2O)]$ (**6**) with view of the coordination sphere of the nickel(II) cation with labeling and displacement ellipsoids drawn at 50 % probability level. The hydrogen atoms were omitted for clarity.

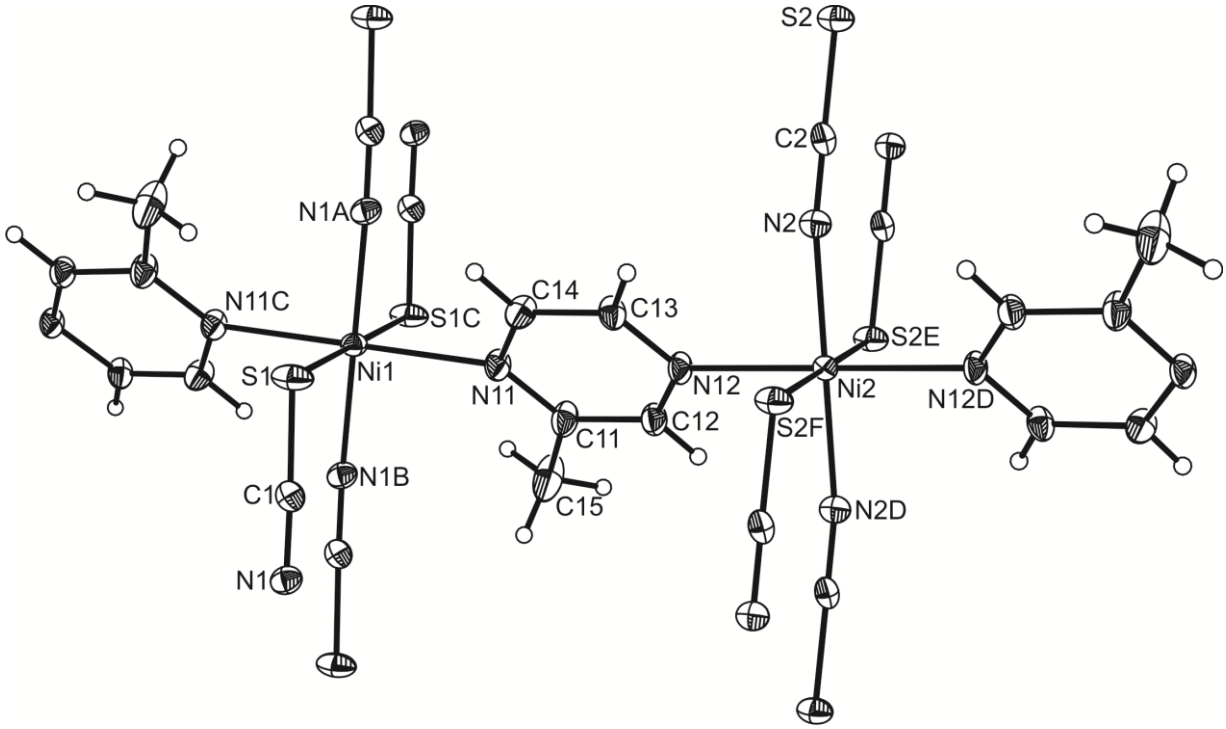

Figure S12. Crystal structure of $[Ni(NCS)_2(2\text{-methylpyrazine})]_n$ (**8**) with view of the coordination sphere of the nickel(II) cation with labeling and displacement ellipsoids drawn at 50 % probability level. Symmetry codes: A = x, y - 1, z; B = -x, -y + 2, -z + 1; C = -x, -y + 1, -z + 1; D = -x + 1, -y + 1, -z + 1; E = -x + 1, -y, -z + 1; F = x, y + 1, z.

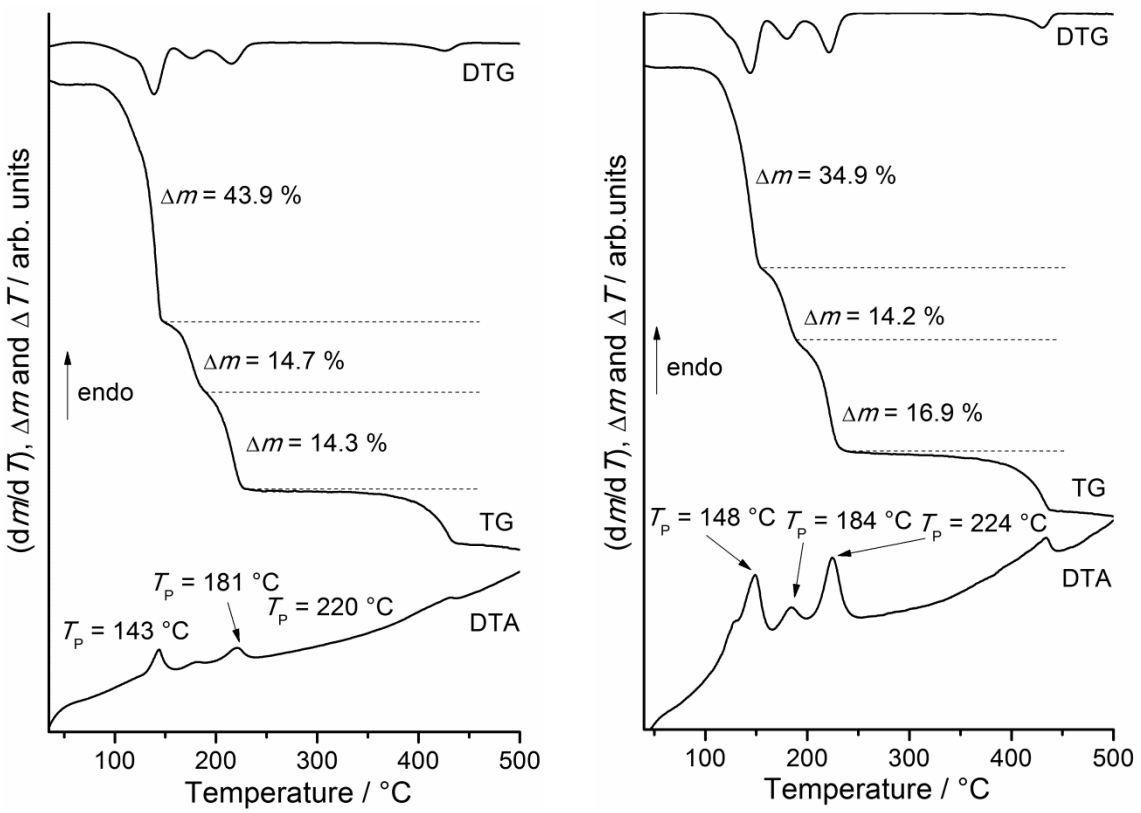

Figure S13. DTA, DTG and TG curves of the ligand-rich 1:5 compounds $Ni(NCS)_2$(2-methylpyrazine)$_4$·2-methylpyrazine solvate (**2**) (left) and $Ni(NCS)_2$(2-methylpyrazine)$_4$·ethanol solvate (**3**) (right). Heating rate = 4°C/min; given are the peak temperatures T_P in °C and the mass loss in %.

Table S1. Experimental and calculated mass losses of the ligand-rich 1:5 compounds: $Ni(NCS)_2$(2-methylpyrazine)$_4$·2-methylpyrazine solvate (**2**) and $Ni(NCS)_2$(2-methylpyrazine)$_4$·ethanol solvate (**3**).

	2		**3**
Δm_{exp} (1. step)	43.9	Δm_{exp} (1. step)	34.9
Δm_{calc} (-3x2-methylpyrazine)	43.8	Δm_{calc} (-2x2-methylpyrazine)	31.50
Δm_{exp} (2. step)	14.7	Δm_{exp} (2. step)	14.2
Δm_{calc} (-1x2-methylpyrazine)	14.6	Δm_{calc} (-1x2-methylpyrazine)	15.7
Δm_{exp} (3. step)	14.3	Δm_{exp} (3. step)	16.9
Δm_{calc} (-1x2-methylpyrazine)	14.6	Δm_{calc} (-1x2-methylpyrazine)	15.7

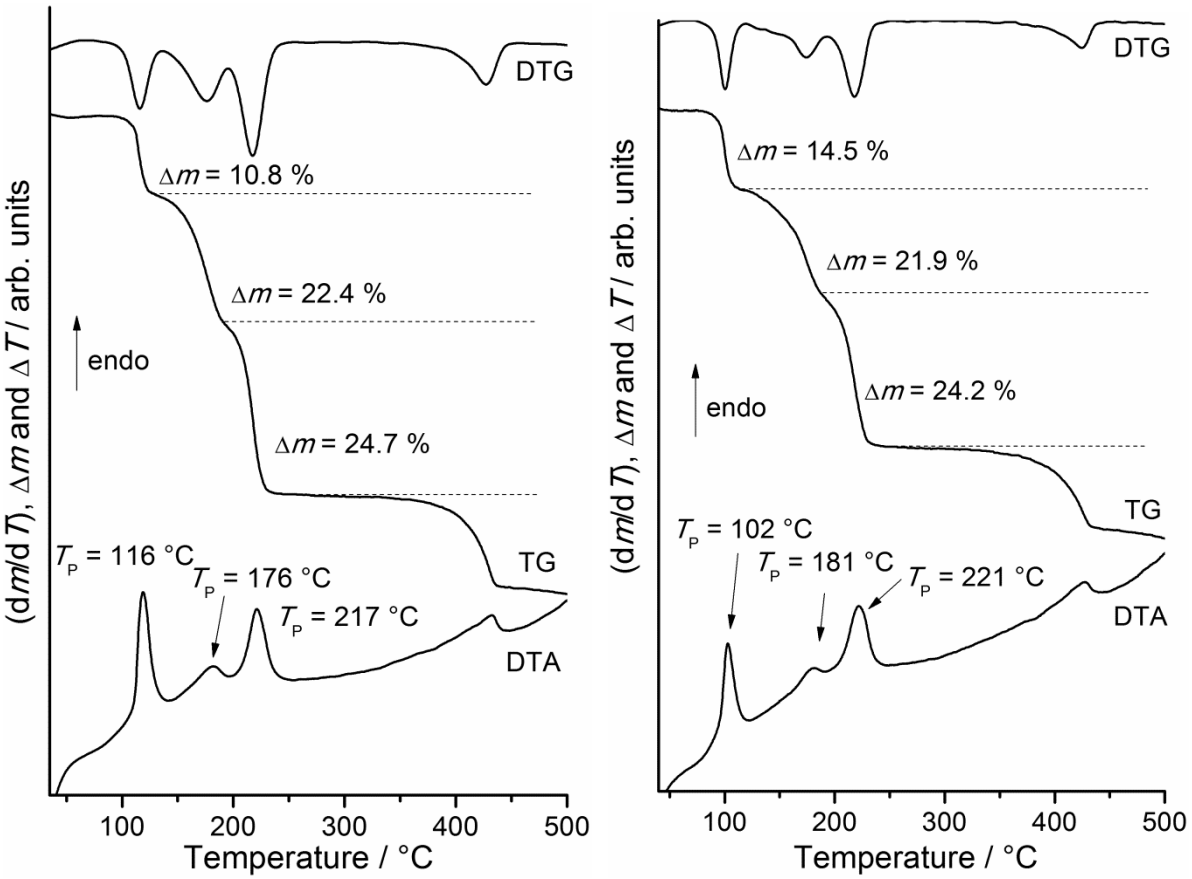

Figure S14. DTA, DTG and TG curves of the ligand-rich 1:2:2 compounds $Ni(NCS)_2$(2-methylpyrazine)$_2(H_2O)_2$ (**4**) (left) and $Ni(NCS)_2$(2-methylpyrazine)$_2(CH_3OH)_2$ (**5**) (right). Heating rate = 4°C/min; given are the peak temperatures T_P in °C and the mass loss in %.

Table S2. Experimental and calculated mass losses of the ligand-rich 1:2:2 compounds: $Ni(NCS)_2$(2-methylpyrazine)$_2(H_2O)_2$ (**4**) and $Ni(NCS)_2$(2-methylpyrazine)$_2(CH_3OH)_2$ (**5**).

	4		**5**
Δm_{exp} (1. step)	10.8	Δm_{exp} (1. step)	14.5
Δm_{calc} (-2 H_2O)	9.01	Δm_{calc} (-2 CH_3OH)	14.9
Δm_{exp} (2. step)	22.4	Δm_{exp} (2. step)	21.9
Δm_{calc} (-1x2-methylpyrazine)	23.5	Δm_{calc} (-1x2-methylpyrazine)	23.5
Δm_{exp} (3. step)	24.7	Δm_{exp} (3. step)	24.2
Δm_{calc} (-1x2-methylpyrazine)	23.5	Δm_{calc} (-1x2-methylpyrazine)	23.5

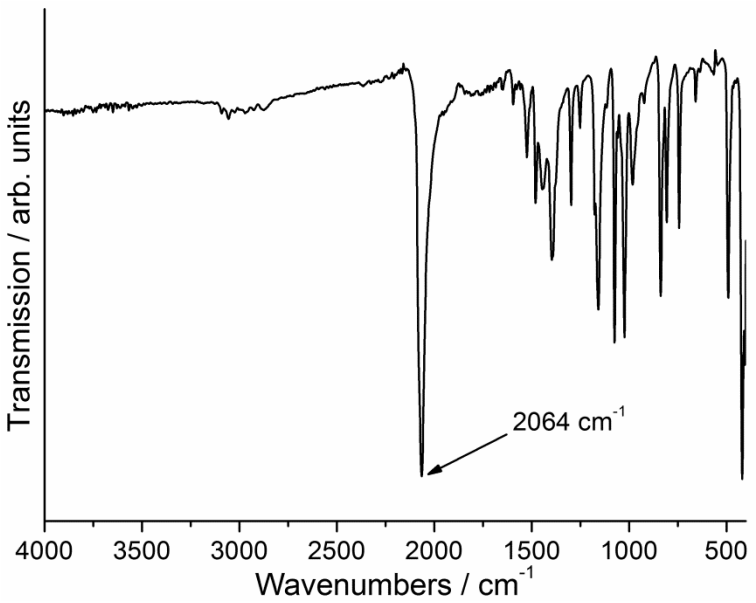

Figure S15. IR spectrum of the ligand-rich compound $Ni(NCS)_2$(2-methylpyrazine)$_4$·2-methylpyrazine solvate (**2**).

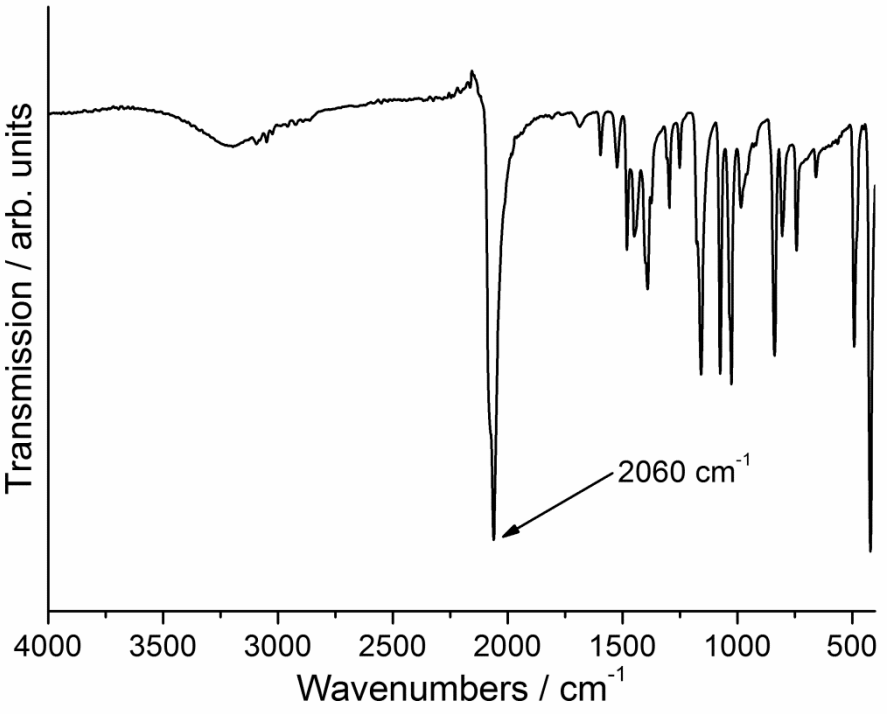

Figure S16. IR spectrum of the ligand-rich compound $Ni(NCS)_2$(2-methylpyrazine)$_4$·ethanol solvate (**3**).

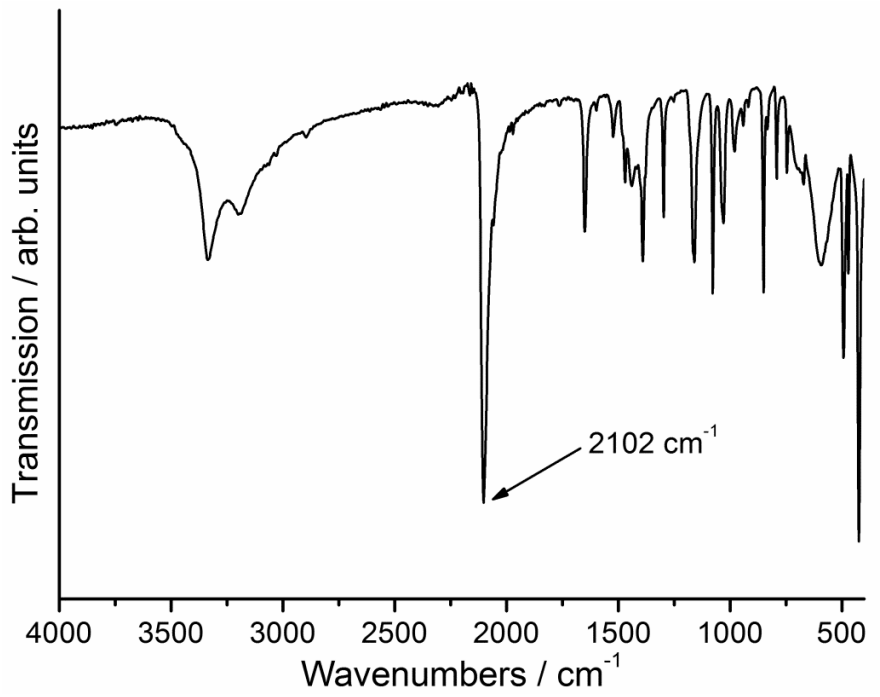

Figure S17. IR spectrum of the ligand-rich 1:2:2 compound $Ni(NCS)_2$(2-methylpyrazine)$_2(H_2O)_2$ (**4**).

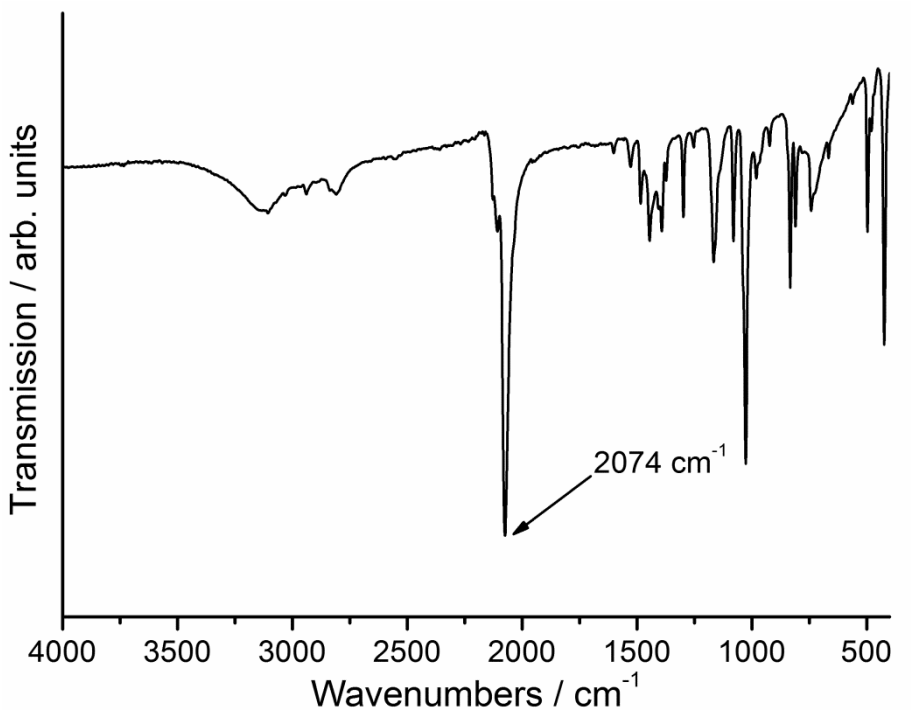

Figure S18. IR spectrum of the ligand-rich 1:2:2 compound $Ni(NCS)_2$(2-methylpyrazine)$_2(CH_3OH)_2$ (**5**).

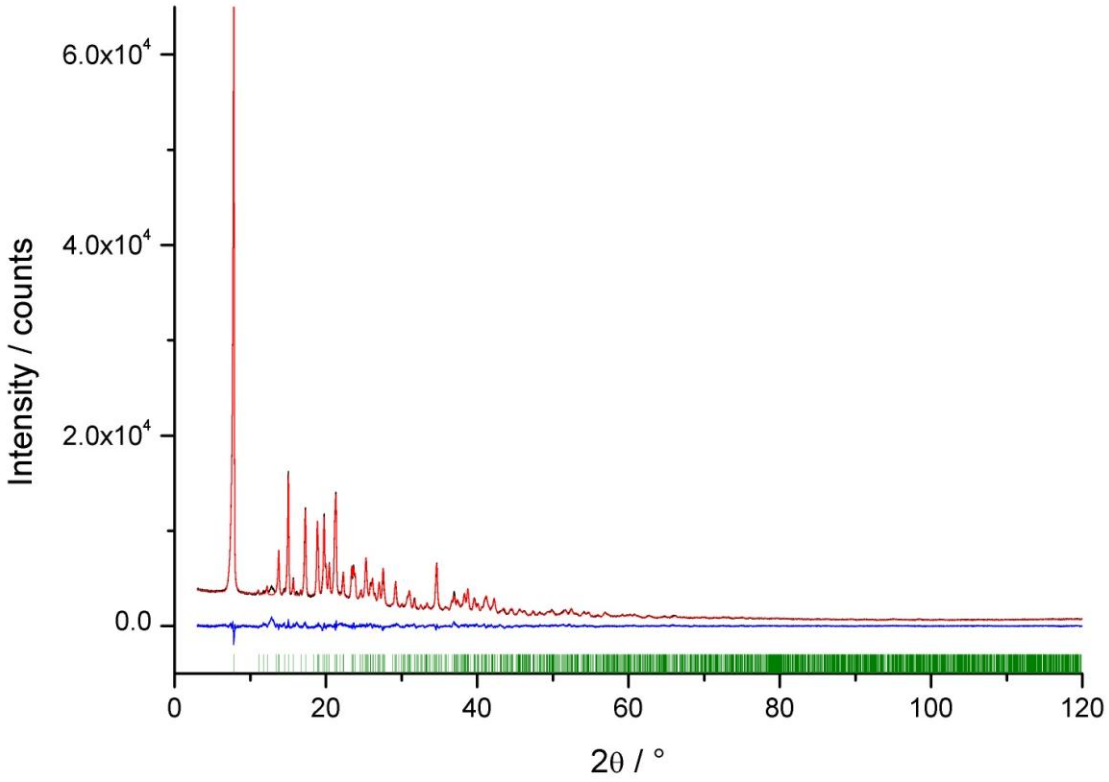

Figure S19. Difference plot of the Rietveld refinement of compound $[Ni(NCS)_2(2\text{-methylpyrazine})_2]_n$ (**7**).

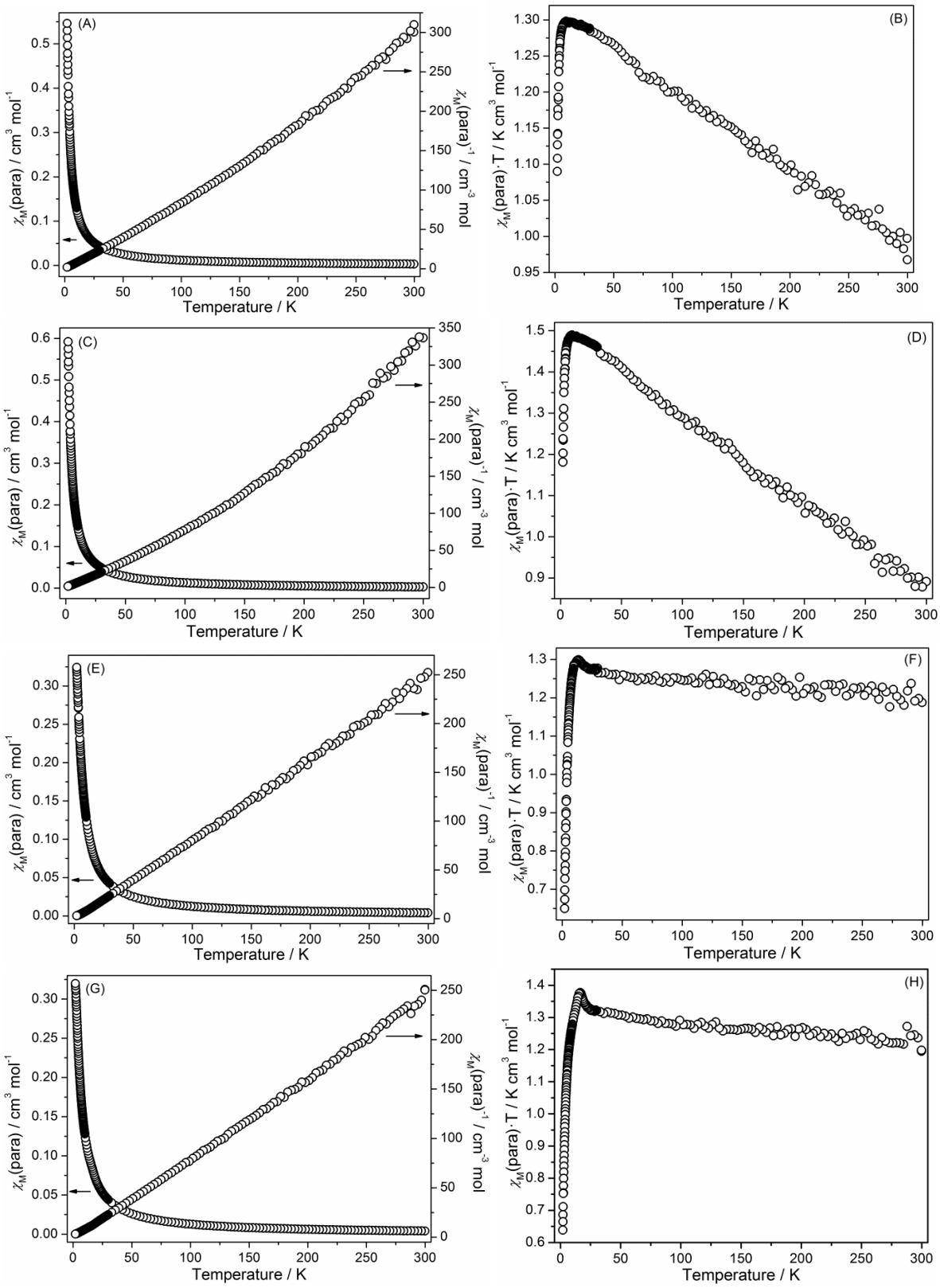

Figure S20. Plots of paramagnetic susceptibility and reciprocal paramagnetic susceptibility (A, C, E, G) and $\chi_M T$ (B, D, F, H) as function of temperature for the 2-methylpyrazine-rich compounds $Ni(NCS)_2$(2-methylpyrazine)$_4$·2-methylpyrazine solvate (**2**) (A, B),[$Ni(NCS)_2$(2-methylpyrazine)$_4$·ethanol solvate (**3**) (C, D), $Ni(NCS)_2$(2-methylpyrazine)$_2(H_2O)_2$ (**4**) and $Ni(NCS)_2$(2-methylpyrazine)$_2(CH_3OH)_2$ (**5**) (E, F) and (G, H).

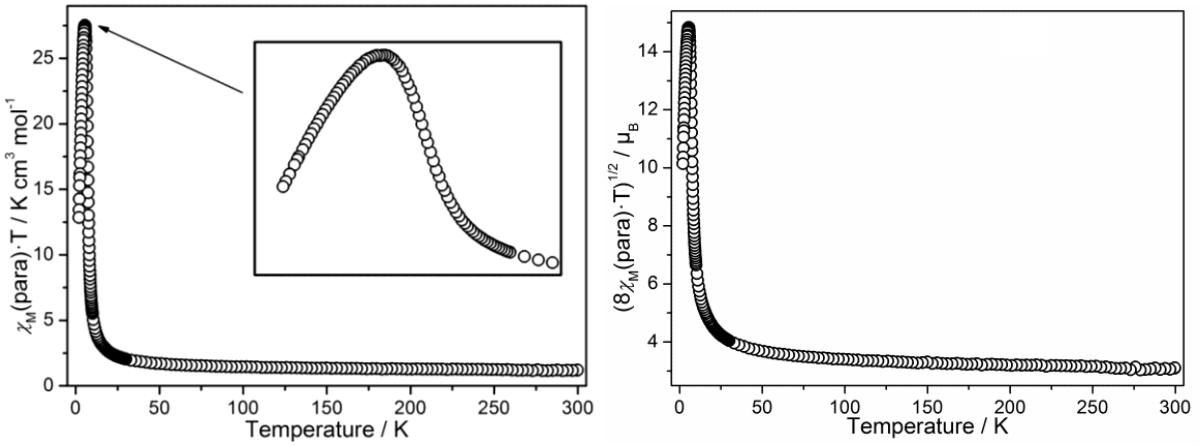

Figure S21. Results of the magnetic measurements for **7**: and $\sqrt{8}(\chi T)$ (left) and χT (right) as function of temperature (at H_{DC} = 1 kOe).

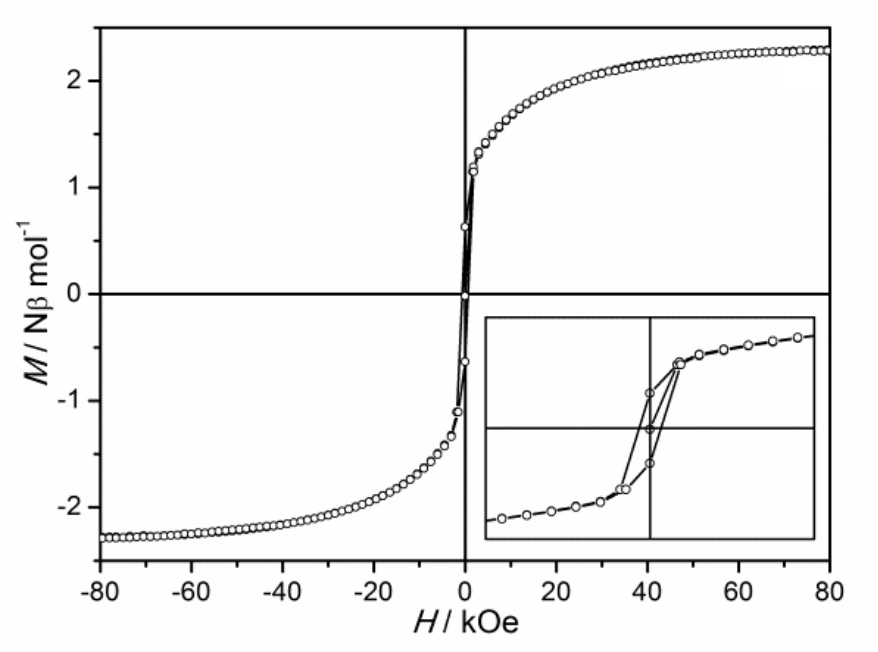

Figure S22. Magnetization experiment at T = 2 K in range of H = ± 90 kOe.

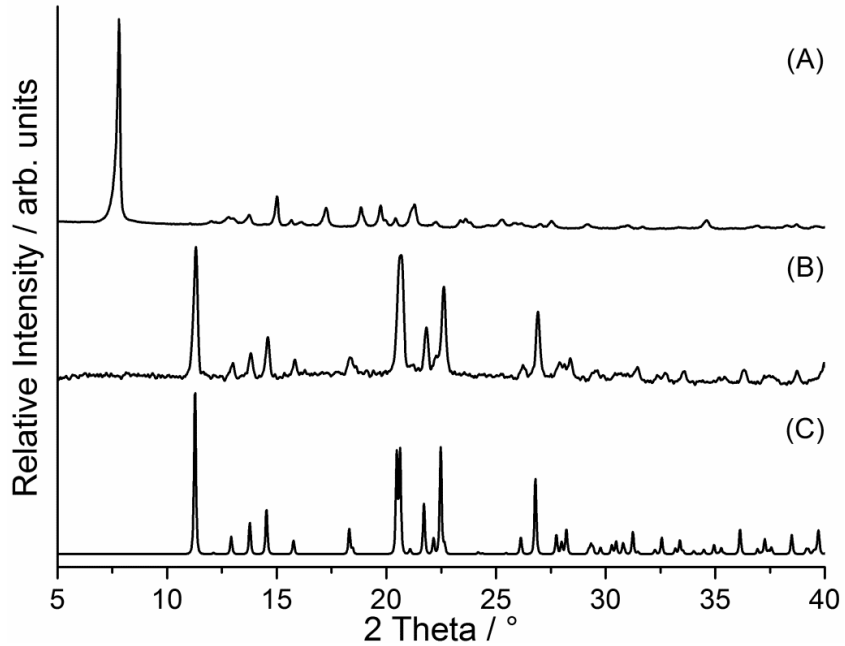

Figure S23. Experimental XRPD of **7** (A) obtained in the first TG step of the thermal decomposition reaction of **4**, which was stored for 1 d in a saturated water atmosphere (B) together with the calculated XRPD of compound $Ni(NCS)_2(2\text{-methylpyrazine})_2(H_2O)_2$ (C).

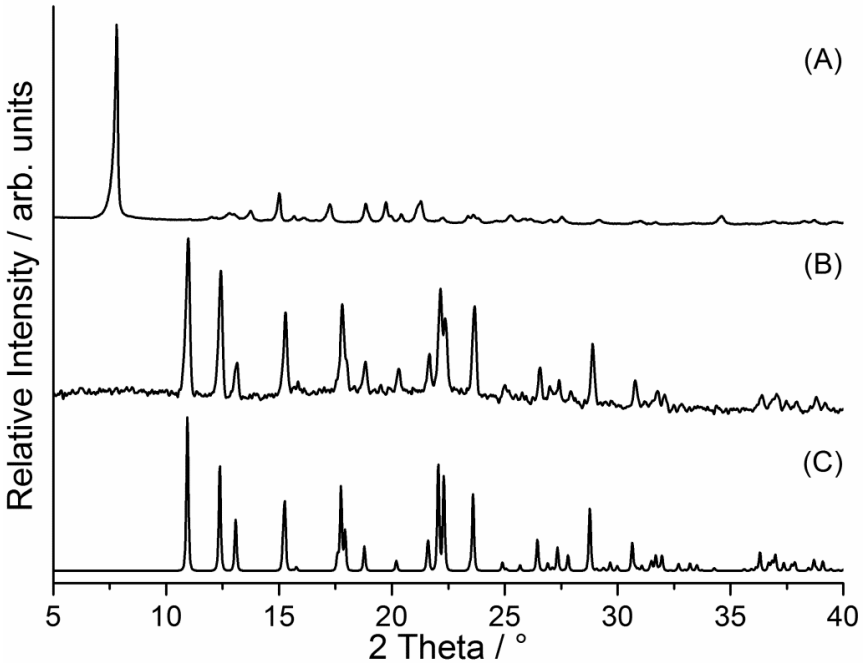

Figure S24. Experimental XRPD of **7** (A) obtained in the first TG step of the thermal decomposition reaction of **5**, which was stored for 1 d in a saturated methanol atmosphere (B) together with the calculated XRPD of compound $Ni(NCS)_2(2\text{-methylpyrazine})_2(CH_3OH)_2$ (C).

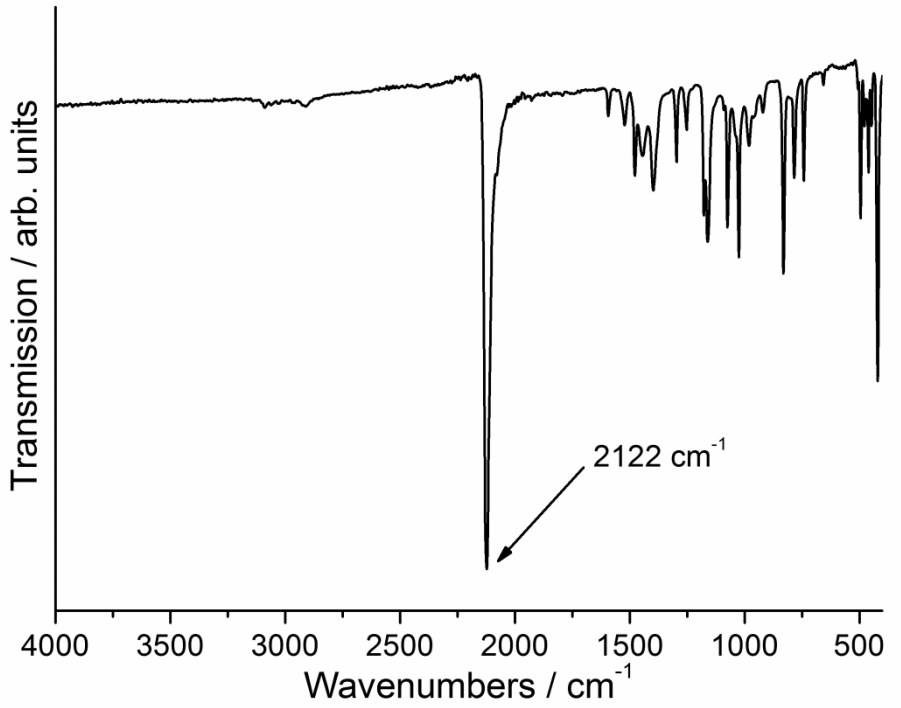

Figure S25. IR spectrum of the residue obtained after the first TG step of the thermal decomposition reaction of **2**.

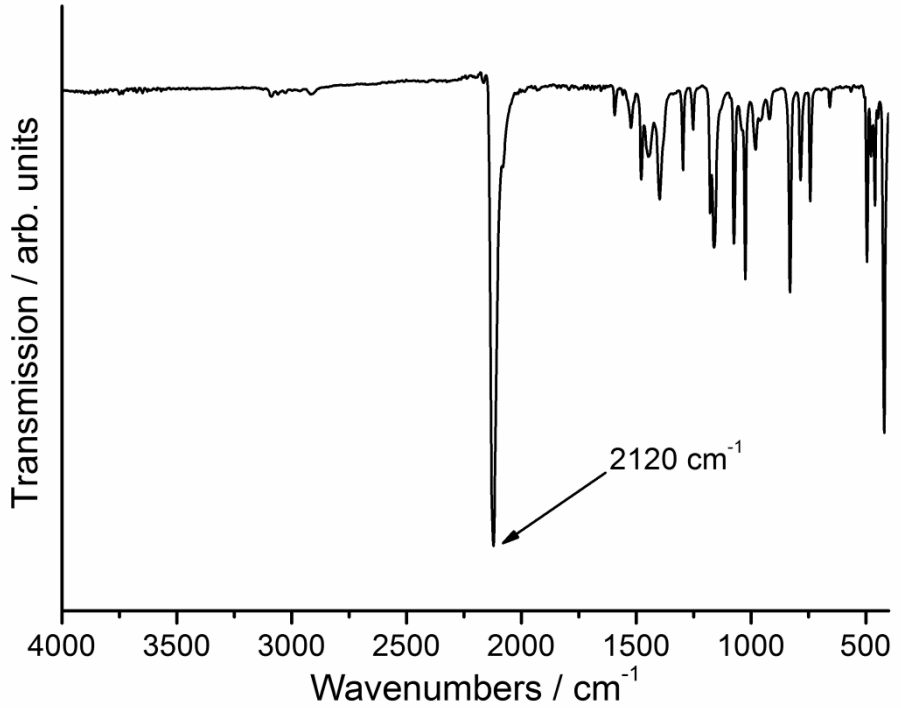

Figure S26. IR spectrum of the residue obtained after the first TG step of the thermal decomposition reaction of **3**.

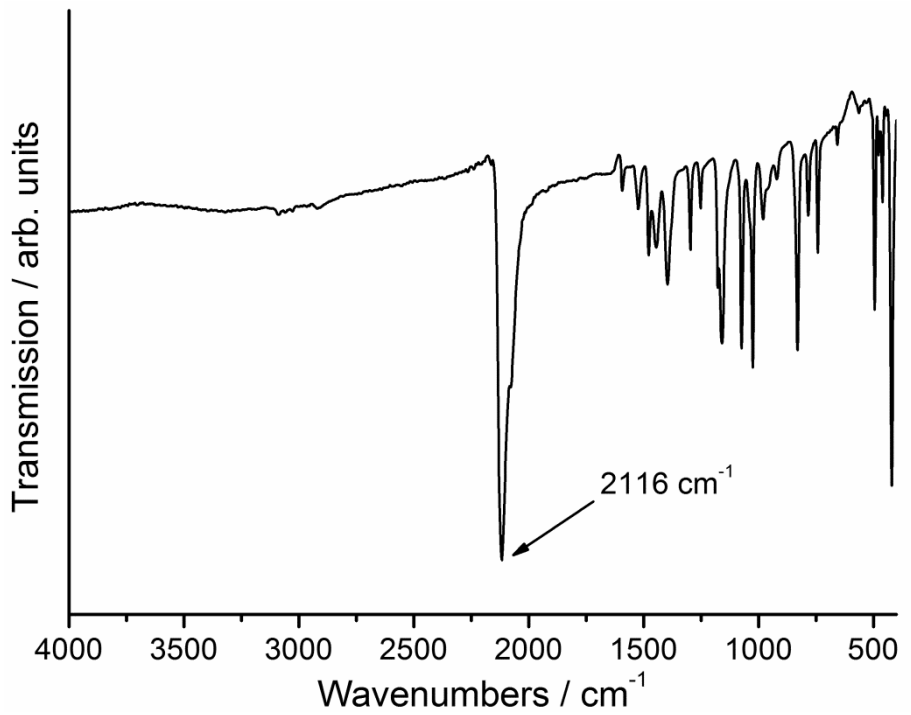

Figure S27. IR spectrum of the residue obtained after the first TG step of the thermal decomposition reaction of **4**.

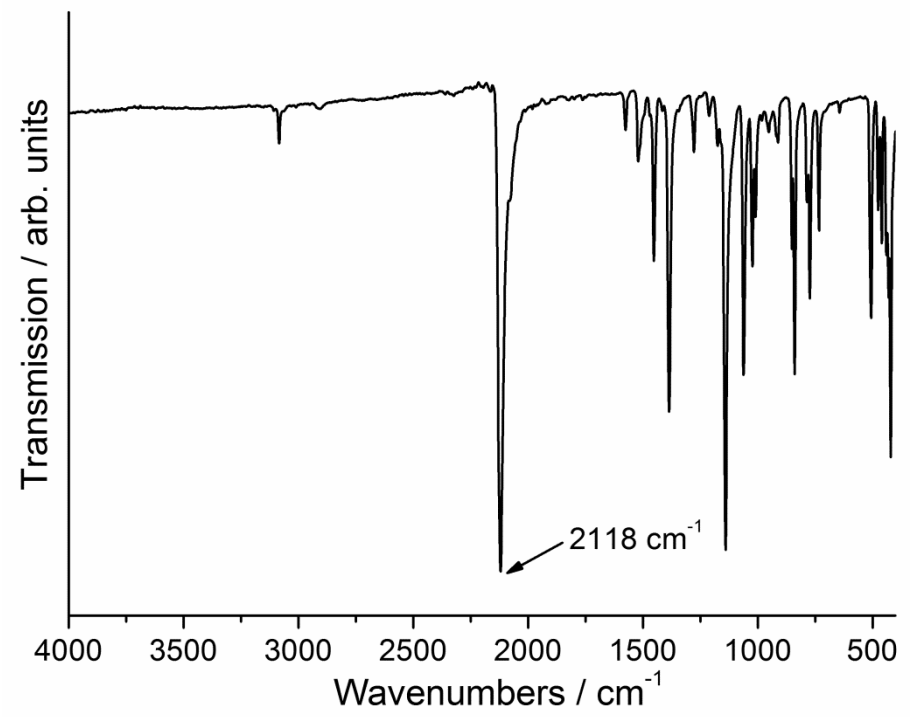

Figure S28. IR spectrum of the residue obtained after the first TG step of the thermal decomposition reaction of **5**.

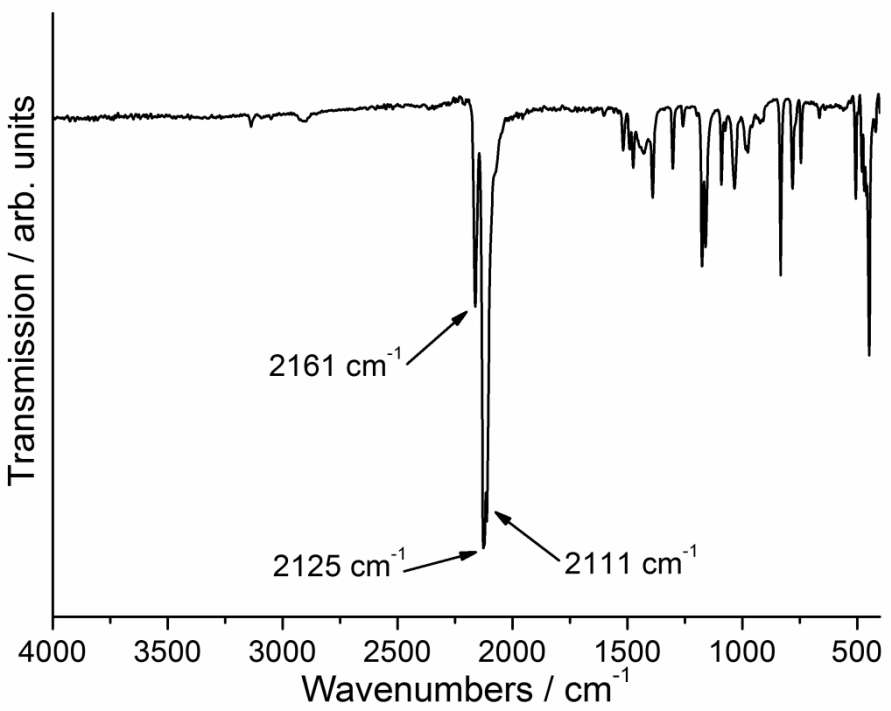

Figure S29. IR spectrum of the residue obtained after the second TG step of the thermal decomposition reaction of **2**.

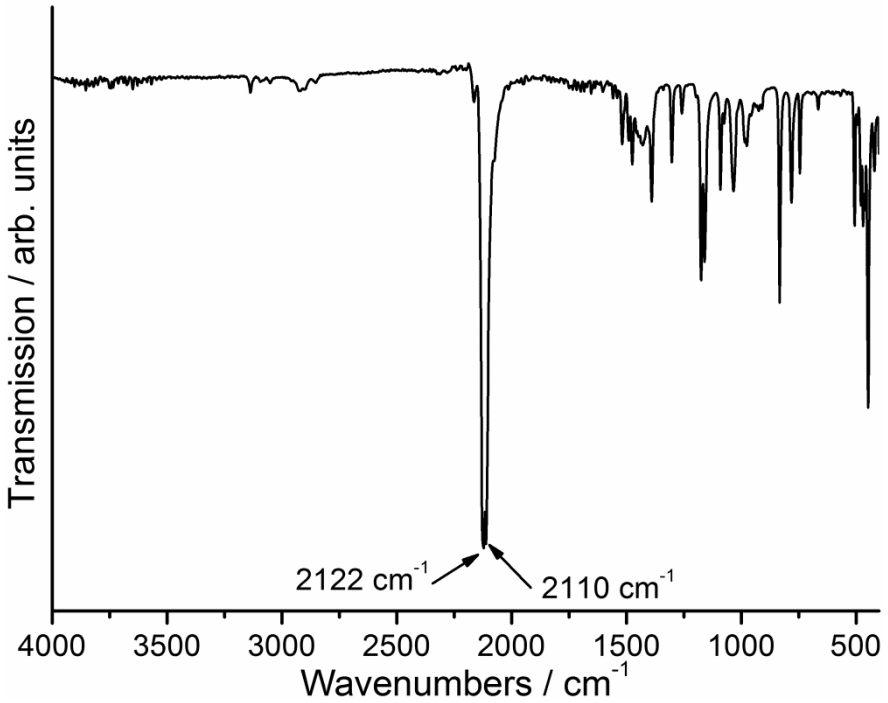

Figure S30. IR spectrum of the residue obtained after the second TG step of the thermal decomposition reaction of **3**.

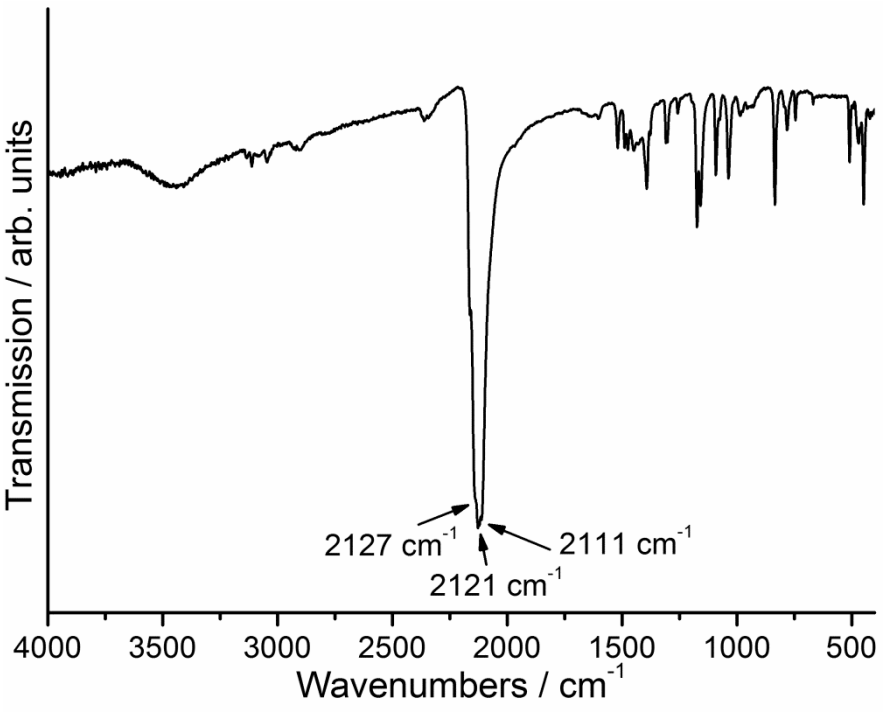

Figure S31. IR spectrum of the residue obtained after the second TG step of the thermal decomposition reaction of **4**.

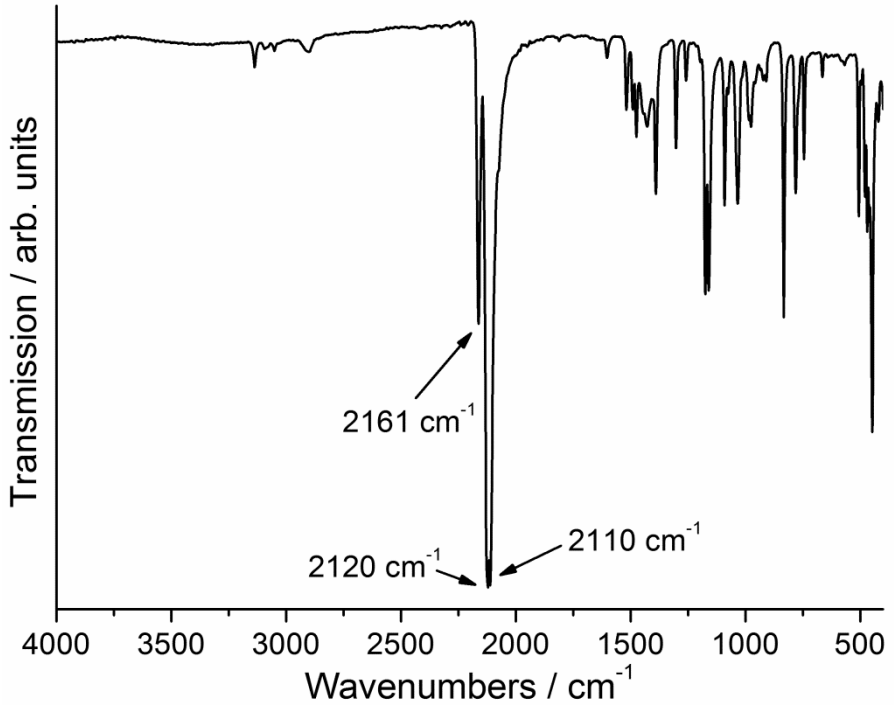

Figure S32. IR spectrum of the residue obtained after the second TG step of the thermal decomposition reaction of **5**.